Journal of Spacecraft and Rockets

VOLUME 7 FEBRUARY 1970 NUMBER 2

A Study of Saturn AS-502 Coupling Longitudinal Structural Vibration and Lateral Bending Response during Boost

R. S. Ryan,* J. G. Papadopoulos,* and L. A. Kiefling*
NASA Marshall Space Flight Center, Ala.

AND

R. Odum,† W. Jarvinen,† and J. Kennoy†
Northrop Nortronics, Huntsville, Ala.

Coupling between lateral and longitudinal oscillations of a launch vehicle can occur as either mass or spring offset. While, in general, mass coupling usually acts through the inertia of the total vehicle, spring coupling acts only through the asymmetrically mounted mass. The Saturn AS-502 space vehicle was analyzed for both types of coupling, with the POGO phenomenon acting as the longitudinal excitation force. Although the mass coupling influence was small, a large lateral acceleration resulted from a spring-type coupling between the ascent and descent stages of the LEM during the latter part of S-IC burn. A response analysis of the vehicle using time-varying coefficients was made and compared with observed flight conditions. The results of this study confirm the necessity of including dynamic cross-coupling mechanisms for adequate prediction of vehicle response. The resulting simulation closely duplicated flight results. The important vehicle parameters involved in creating the lateral/longitudinal coupling phenomenon were studied.

Introduction

USUALLY space vehicles are built with an external geometric symmetry, but contain internal mass offsets and show structural asymmetries. If these asymmetries are small, the design engineer may treat the oscillatory modes in the separate planes as uncoupled. Occasionally, this simplification is not permissible because coupling between the various modes creates large local loads. The creation of these high loads requires a coupling mechanism, a forcing function in one of the directions, and sharp tuning of the characteristic frequencies of the system.

The recent Saturn AS-502 vehicle test flight exhibited a strong dynamic coupling phenomenon between longitudinal and lateral oscillation modes with large local loads in the spacecraft region. Postflight analysis showed that the three necessary conditions for creating these loads were met: the mounting between the LEM ascent and descent stages is unsymmetrical creating a spring-mass offset type of coupling mechanism; a pronounced closed loop longitudinal/propulsion system oscillation (called POGO) that became unstable and acted as the forcing function to the lateral LEM mode; and the lateral LEM mode frequency was in resonance with POGO providing the sharp tuning between modes of oscillation. The POGO produced a longitudinal acceleration on the LEM of 0.72 g which was superimposed on the steady-state vehicle acceleration load of 3.7 g. The 0.72 g longitudinal acceleration occurring at approximately 5.3 Hz produced a lateral acceleration in the LEM of 0.65 g at 5.3 Hz. Loads of this magnitude are reaching the danger limit, and had not been predicted before flight. Since all prior analyses considered only one oscillation plane at a time, a technique was needed that could quickly and accurately explain the phenomenon observed in flight.

The basic philosophy chosen is to simplify the system to include only the essential elements in a general representation and study the sensitivity of the vehicle responses to pertinent parameter variations.

Forcing Function (POGO)

The vehicle structural oscillations can be represented as a simple spring-mass model obtained from a detailed lumped mass model. The displacement of the vehicle in any one of these modes can be written as

$$\ddot{q}_i + 2\zeta_i\omega_i\dot{q}_i + \omega_i q_i = X_{Ti}T'/M_i \qquad (1)$$

Presented as Paper 69-58 at the AIAA 7th Aerospace Sciences Meeting, New York, January 20–22, 1969; submitted February 5, 1969; revision received August 22, 1969.

* Aerospace Engineer. Member AIAA.

† Aerospace Engineer.

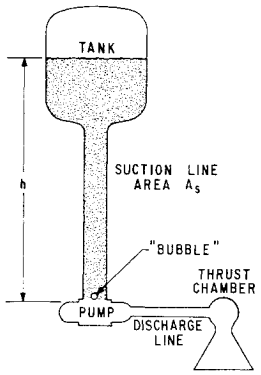

Fig. 1 Schematic of propulsion system.

where q_i is the generalized displacement ω_i the generalized frequency, ζ_i generalized damping, M_i generalized mass, X_{Ti} the modal displacement at the force application, and T' the force. The displacement or acceleration of any point on the vehicle can be formulated using the generalized displacement and corresponding mode shape value for the desired station. The displacement at any point r is

$$x(rt) = q_i(t)\, X_i(r) \tag{2}$$

Structural vibrations act on the propellant tank bottom producing perturbations in the fluid which result in oscillatory pressure at the top of the suction line (tank bottom). To represent this pressure fluctuation, the effect of flow in the tank is neglected, because of the large diameter of the tank relative to that of the suction line. Pressure perturbations in the gas above the propellant have also been neglected. Therefore, pressure = force/area, or

$$P_t = h(t)\ddot{q}_i(t)X(x)\rho/g \tag{3}$$

where ρ is the propellant weight density, $h(t)$ the height of propellant in the tank, and q_i and X the generalized coordinate and deflection as defined previously.

The suction line, which carries propellant from the tank to the combustion chamber, acts as a conductor for the pressure and flow rate disturbances originating at the tank bottom (Fig. 1). The speed (acoustic velocity) at which pressure disturbances are propagated through a compressible fluid in an elastic pipe is a function of the fluid bulk modulus (compressibility), elastic modulus (Young's modulus) of the pipe material, the pipe diameter, the pipe thickness, the fluid density, and the pipe mounting (restrained ends, unrestrained ends, etc.). The fundamental or first "organ pipe" frequency of acoustic wave propagation in the suction line can be expressed as

$$f = C_0/\lambda \tag{4}$$

where C_0 = acoustic (wave) velocity of a compressible fluid in an elastic pipe, in./sec; f = frequency, cps; and λ = wavelength, in. Making use of this acoustic property, the expressions for the pressure and flow rate at the pump inlet end of the suction line are

$$P_a = \alpha P_b + (LS + R)\beta\dot{w}_b \tag{5}$$

$$\dot{w}_b = (CS)\beta P_a + \alpha\dot{w}_a \tag{6}$$

where $\alpha \equiv 4LCS^2/\pi^2 + RCS/2 + 1$; $\beta \equiv LCS^2/\pi^2 + RCS/6 + 1$; P_j = suction line pressure, lb/in.^{2}; $\dot{w}_j$ = suction line weight flow rate, lb/sec (j = a,b: a = upstream, b = pump inlet); and C, L, and R = line segment capacitance (in.^{2}), inductance (sec^2/in.^{2}), and resistance (sec/in.^{2}), respectively. These transfer functions depict the amplitude and phase angle of pressure and flow rate at the terminals of a uniform duct and are accurate up through the first mode frequency [$\omega_n = \pi/2\ (LC)^{1/2}$]. To determine the effects of higher modes (not needed in this simplified analysis), these equations may be reapplied to the duct by considering it to be composed of individual segments of shorter length, with Eq. (5) used for each segment. Using appropriate boundary conditions between each segment and solving the resulting simultaneous set of equations yields a transfer function for the total feedline containing the desired higher frequencies.

For systems where the first organ pipe mode frequency is much higher than other oscillatory mode frequencies a simpler expression exists, subject to the following assumptions: 1) $\dot{w}_a = \dot{w}_b$ (line capacitance is neglected), and 2) $R' = 0$ (fluid resistance is neglected in view of much larger downstream resistances). Equation (5) then becomes

$$P_a = P_b(LS)\dot{w}_b \tag{7}$$

The flow rate through the pump is a flow relative to the pump, and therefore, the inertial flow rate, described by Eqs. (5) and (6), must be converted into a relative one by the following equation:

$$\dot{w}_{\text{relative}} = \dot{w}_{\text{inertial}} + \rho A_p\left[\sum_{i=1}^{N} q_i(t)X(x)\right] \tag{8}$$

where A_p is the cross-sectional area of the pump inlet, and the bracketed summation is the perturbative longitudinal velocity of the pump.

The analysis of the Saturn V system requires the application of the above equations to represent both the fuel and LOX suction lines. Since four of the five engines swivel, the four swivel-engine LOX suction lines can be lumped into one set, with the center engine LOX line treated separately. The fuel suction lines can be lumped into one model since the lines are much shorter than the LOX sucton lines.

Engine System Dynamics

The engine system is composed of 1) the pumps, 2) the discharge lines, and 3) the thrust chamber. Most investigators have analytically described each of the engine system components, considering operating characteristics of each subsystem.[1,2] However, because of the availability of experimental data for the total F-1 engine system, the transfer function derived from these data is considered to be a better representation for over-all system dynamics.[3,4] These equations are

$$P_{js} = [A_j + B_j(t)/S]\ [\dot{w}_{js} - \dot{w}_{jd}] \tag{9}$$

$$F = (\partial f)/(\partial P_{js})P_{js} + (\partial f)/(\partial P_{fs})P_{fs} \tag{10}$$

$$\dot{w}_{jd} = (\partial\dot{w}_{jd})/(\partial P_{js})P_{js} + (\partial\dot{w}_{jd})/(\partial P_{fs})P_{fs} \tag{11}$$

where A_j = "cavitation" resistance, sec/in.^{2}; $B_j(t)$ = "cavitation" compliance, 1/in.^{2}; P_{js} = suction line pressure at pump, lb/in.^{2}; $\dot{w}_{js}$ and $\dot{w}_{jd}$ are weight flow rates at the pump (suction), and in the discharge line into thrust chamber (lb/sec), respectively; and F = F-1 engine thrust, lb; and where j = O,f: oxidizer, fuel. Reference 3 refers to B_0 and B_f as cavitation compliances; however, subsequent investigation indicates that a portion of this suction line resonance may be attributed to dynamics associated with the pressure-volume compensator. Whatever the source, the empirical results from component test data should represent the physical system dynamics.

The total force on the structure is the resultant of the upward F-1 engine thrust acting at the gimbal plane, described by the previously mentioned transfer functions, and the downward suction force acting on the pump. Assuming that these suction forces act at the gimbal plane, then

$$T = F + A_{js}P_{js} + A_{fs}P_{fs}, \tag{12}$$

where T = total force due to F-1 engine, lb; and A_{js} and A_{fs} are the suction line cross-sectional areas at the pump inlet for oxidizer and fuel, respectively, in.^{2}

Accumulator Dynamics

There have been several approaches to eliminating the POGO instability. The one chosen for the Saturn vehicle is the installation of an accumulator in the LOX suction line prevalve. These devices are similar in operation to the surge tanks used in water hammer problems. They serve as a point of pressure relief or cushion whenever there is a change in pressure or flow. The dynamics of the accumulator are described by

$$\dot{w}_A = \frac{(\rho_0/K_A)\, SP_A}{(\rho_0 L_A/K_A)S^2 + (\rho_0 R_A/K_A)\, S + 1} \tag{13}$$

and

$$\dot{w}_b = \dot{w}_a - \dot{w}_A;\ P_b = P_A = P_a \tag{14}$$

where L_A, R_A, and K_A are the inertance, linear resistance, and spring rate of the accumulator duct, respectively.

Coupling Mechanism

There are basically two types of couplings predominant in launch vehicles. The first is a symmetrically arranged mass whose supporting structure is unsymmetrical to the shell structure of the vehicle. This is referred to as a spring offset. The second is a mass which is not located on the vehicle centerline.

Three methods for deriving the equations of motion for a three-dimensional system with internal spring-mounted masses (LEM) were considered. The best one computes over-all three-dimensional structural modes and frequencies by representing the structural modes as lumped mass and springs. Although the most desirable, it requires much analysis and computer time not available initially for this study. However, the results using this approach became available at the end of the analysis and were used as verification of results obtained. A second approach calculates the planar modes of the vehicle with the internal spring-mounted mass considered rigid. The effects of the coupling and the spring mounting are accounted for by writing additions representing these coupling modes and solving them simultaneously with the original over-all mode equations. The third approach assumes the over-all system modes to be calculated for each plane without the internal spring-mounted mass. The effect of this mass and its mounting is represented by an additional set of equations that are solved simultaneously with the over-all structural equations. Because of the availability of basic data in the form of planar

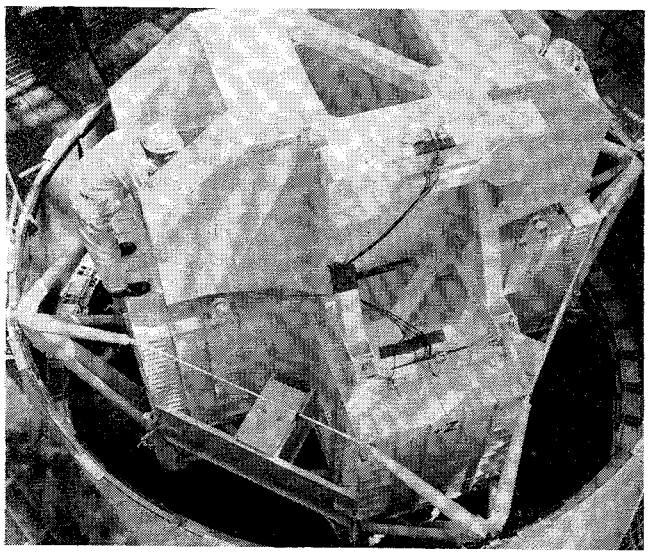

Fig. 2 Saturn V LEM.

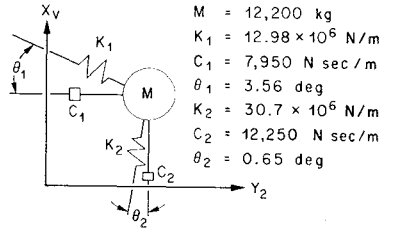

Fig. 3 Two-degree-of-freedom LEM model determined from a 43 degree-of-freedom model.

modes and the absence of significant coupling in the yaw plane, the second approach was used in this analysis.

Using the structural characteristics data computed for the planar case (LEM rigid), we can calculate the vehicle response in any mode from

$$\ddot{\eta}_{B\mu} + 2\zeta_{B\mu}\,\omega_{B\mu}\,\dot{\eta}_\mu + \omega^2{}_{B\mu}\eta = Q_\mu/M_{B\mu} \tag{15}$$

where η_μ is the generalized coordinate; $\zeta_{B\mu}$, $\omega_{B\mu}$, $M_{B\mu}$ are the generalized damping, frequency and mass; and Q_μ is the generalized force.

To obtain the effect of the cross-coupling due to the off-center spring-mounting of the LEM (Lunar Excursion Module), a detailed model of the LEM ascent and descent stages and the connection at the SLA (Service Module Lunar Adapter) interface was made using 43 degrees of freedom. Figure 2 shows the connection between the LEM ascent and descent stage and illustrates the stiffness eccentricity of the structure.

The 43-degree-of-freedom system is solved to determine the elastic modes and the equivalent spring mass analog system. A model containing the first two uncoupled modes (Fig. 3) was used for the following simulation. This model represents the longitudinal and pitch degrees of freedom of the LEM. The yaw degree of freedom can be omitted because of structural symmetry considerations.

To include the effects of the LEM dynamics and cross-coupling, Eq. (15) must be modified to account for the additional forces acting on the structure. This modification yields the general representation for each planar mode (longitudinal or lateral) as

$$\ddot{\eta}_\mu + 2\zeta_{B\mu}\omega_{B\mu}\dot{\eta}_\mu + \omega_{B\mu}{}^2\eta_\mu = \frac{F_x Y_\mu(L,S)}{M_B} + \frac{TY_\mu(X_T)\beta}{M_{B\mu}} \tag{16}$$

and

$$\ddot{q}_i + 2\zeta_i\omega_i\dot{q}_i + \omega_{Bi}{}^2 q_i = \frac{TX_i(\tau)}{M_i} + \frac{F_x X_i(L,S)}{M_i} \tag{17}$$

with additional equations required for the lateral and longitudinal LEM modes:

$$\ddot{x} + (K_{11}/m)x + (K_{12}/m)y + (C_1/m)\dot{x} + \Sigma\, \ddot{q}_i X_i\,(L,S) = 0 \tag{18}$$

and

$$\ddot{y} + (K_{22}/m)y + (K_{21}/m)x + (C_2/m)\dot{y} + \Sigma\, \ddot{\eta}_u Y_i\,(L,S) = 0 \tag{19}$$

The forces F_x and F_y acting on the structure are the damping and spring force obtained from Eqs. (16) and (17):

$$F_x = (C_1/m)\dot{x} + (K_{11}/m)X \tag{20}$$

and

$$F_y = (C_2/m)\dot{y} + (K_{22}/m)Y \tag{21}$$

where x and y are the relative longitudinal and lateral displacement coordinates of the LEM generalized mass.

Use of Eqs. (18–21) allows the representation of the vehicle structural characteristics including cross-coupling and an elastic internal mounted mass. To account for mass coupling, the eccentricity of mass offset from the vehicle centerline must be multiplied by the acceleration and its lever arm to obtain

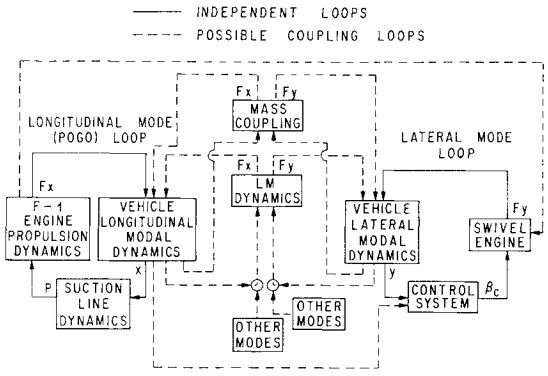

Fig. 4 Block diagram of longitudinal and lateral system.

a moment acting on the vehicle. The mass coupling term between any longitudinal mode and any lateral mode (flexible or rigid) is

$$T_{ij} = \int_l m'(x)\mu j(x)\omega_i'(x)\bar{Z}(x)dx \qquad (22)$$

where x is the longitudinal coordinate, l is the vehicle length, m' is the mass per unit length, ω is the longitudinal modal displacement, ω' is the bending modal slope, $\bar{Z}$ is the distance from the vehicle center to the elemental mass center. Because of the small effect of these mass offset terms on the present Saturn V, less than 2% of the diagonal terms, they are considered negligible in this analysis.

Control System (Lateral)

The control system, which is a potential second order cross-coupling mechanism from lateral to longitudinal, consists of various sensors, shaping networks designed for bending mode stability, and servo-actuators. Control of the vehicle is maintained by swiveling the engines, using a hydraulic actuator for positioning. The actuator position is determined from a control law formulated to produce desired response and stability. The control law results from a proper choice of gains attached to the output signal from various control sensors whose signals are summed and fed directly to the actuators.

The control law is formed using the signals from the control sensors which are vehicle attitude (φ_i) and rate ($\dot{\varphi}_R$), superimposed with proper gains, a_0 and a_1.

$$\beta_c = a_0\varphi_i T_1(S)A(S) + a_1\dot{\varphi}_R T_2(S)A(S) \qquad (23)$$

Sensor dynamics are included in the equations of motion of the total system. Shaping networks, introduced for stability consideration and indicated as $T_i(S)$, represent the transfer function between signal input and output. The actuator transfer function is indicated by $A(S)$.

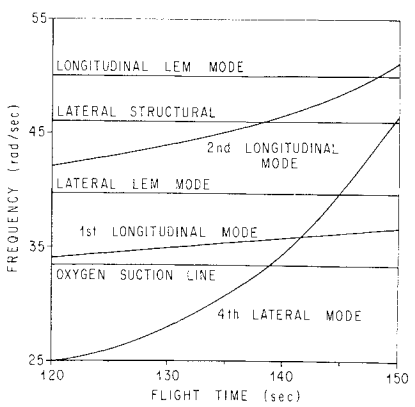

Fig. 5 Uncoupled system frequency characteristics.

Combined System Simulation

In Fig. 4, the POGO and lateral mode loops are the major blocks. These two systems are coupled with the spring coupling of the LEM. Additional potential coupling is shown in dotted lines for mass offset coupling and the secondary effect of longitudinal thrust resulting from swiveling the engines laterally. Since all the couplings except the LEM spring coupling are negligible, only this effect is included in the analysis.

The resulting system contains: 1) the first two longitudinal modes of the space vehicle with 0.9% critical damping; 2) the first two modes of LOX suction lines, and the first mode of fuel suction lines; 3) the Rocketdyne transfer functions for the F-1 engines; 4) the first five lateral pitch bending modes of the space vehicle with 1% critical damping (reduced to fourth and fifth modes for some studies); 5) pitch control system (yaw not in due to symmetry considerations); 6) swivel engine pitch deflection; 7) prevalve accumulators (when needed); 8) first LEM coupled pitch mode; 9) first LEM coupled longitudinal mode. Time-varying coefficients were used for all modal characteristics and fuel heights.

Two methods were used to solve this set of equations for the vehicle responses: numerical integration of the describing differential equations on a digital computer, and integration of differential equations on an analog computer. The digital approach offers more accuracy and model details, while the analog allows speed of solution. Since many parameter variations were needed for sensitivity considerations, the analog was used for most studies with the digital results serving as a base for checks.

Simulation Results

To better assess the simulation results obtained, the Saturn AS-502 flight records were evaluated in detail. Telemetry data from the lateral control system revealed that the control rate gyros measured a 5.3 Hz POGO oscillation, but the control system filters removed this frequency by attenuation. Therefore, pitch and yaw engine positions were devoid of 5.3 Hz perturbation. The conclusion can be drawn that the lateral control loop produced no significant effect in the 5.3 Hz range.

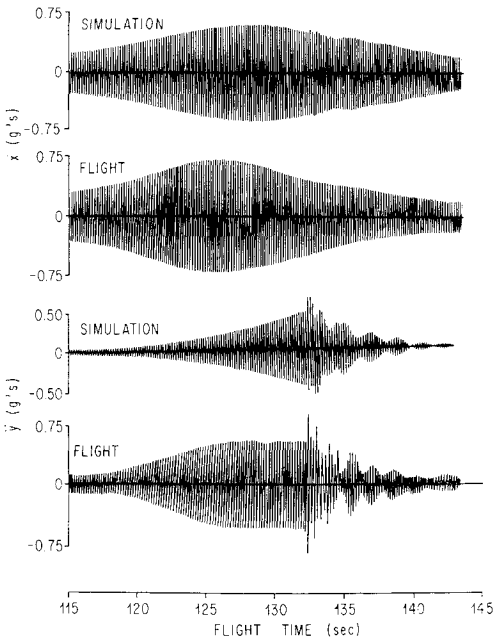

Fig. 6 Comparison of simulation AS-502 flight results for lateral and longitudinal LEM accelerations.

A study of slosh frequencies during S-IC burn indicates no predominant slosh frequency above 1.3 Hz. These facts combine to indicate that the lateral accelerations experienced during POGO were due to a structural coupling between the longitudinal vibration and the lateral bending modes of the vehicle.

In Fig. 5, the analytical calculated uncoupled frequencies of the system show the potentially dangerous resonance conditions between propulsion system, longitudinal modes, and lateral LEM mode; and the analytical calculated coupled frequencies show the strong interaction. The close proximity of the first longitudinal modal frequency with that of the LOX suction line occurs in the 110 to 120 sec region, causing the largest decrease in stability margin. This decrease in stability margin or in system damping results in divergence at the longitudinal response. In the period from 120 to 150 sec, the longitudinal modal frequency and the LOX suction line resonant frequency are drawing apart, resulting in an increase in system stability and a converging of system response, as seen in Figs. 6–8. The longitudinal LEM mode would be excited by this first longitudinal mode response; and whereas the longitudinal LEM mode is not in resonance with the first longitudinal mode, it still conveys energy and response into the lateral LEM mode through the coupling mechanism. Figure 5 indicates that the lateral LEM mode resonant frequency coalesces with the first longitudinal modal frequency in the period between 130 and 140 secs. Thus, a buildup of LEM lateral response should be expected during this time, since it is being forced at its resonant frequency. Figure 6, presenting the longitudinal ($\ddot{x}$) and lateral ($\ddot{y}$) accelerations of the LEM from the simulated and actual AS-502 flights, shows that this tuning does occur.

The first simulation results matched the flight results until 133 sec flight (not shown), but did not show a sharp spike in the lateral LEM response at 133 sec and the resulting beat that followed. A study of the flight data shows a 10% shift in LEM frequency at 133 sec. Based on the flight data, a corresponding LEM frequency shift was introduced into the simulation, producing the results shown. The comparison with the flight is good with the peak values approximately equal, although the modal coupling does not occur quite as early as in actual flight. The shifting of the LEM lateral frequency produced the correct beat frequency. Motion picture film of the flight indicates that a portion of the SLA panel failed at this flight time. This panel failure could possibly explain the frequency shift. As yet, analysis does not show a frequency shift of 10%, but more on the order of 4 or 5%. Unknown conditions could account for the rest of the shift.

The sensitivity of the system to parametric variations can be inductively determined. Any low-damped, sharply tuned system is very sensitive to frequency, damping, and influence coefficient changes. Although the basic trends can be predicted, the picture is somewhat clouded by the possible energy exchange caused by the coupling mechanism in the LEM. Therefore, a parametric sensitivity investigation was conducted. Figure 7 is a half envelope plot of longitudinal and lateral LEM acceleration for varying the longitudinal modal frequency by plus and minus 10%. Increasing the frequency basically eliminates both longitudinal and lateral oscillations, while decreasing the frequency reduces the longitudinal oscillations by a factor of 4 and eliminates the lateral oscillation. An examination of Fig. 5 shows that this should occur. As the first longitudinal modal frequency is raised, it is no longer in close proximity with the LOX suction line resonant frequency at a time when modal mass and influence coefficients are critical. Therefore, the POGO disappears, and without its forcing function, the lateral response does likewise.

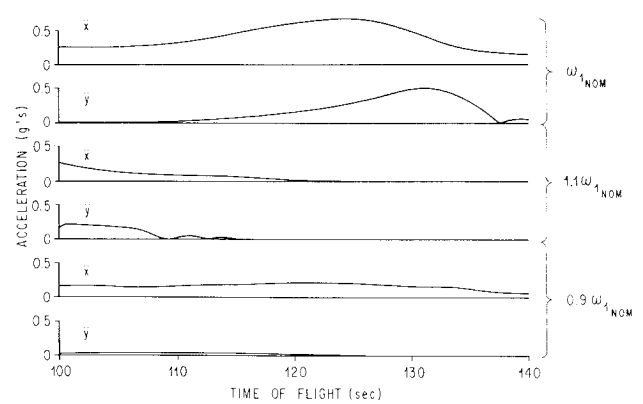

Fig. 7 Effect of varying first longitudinal modal frequency on lateral and longitudinal accelerations of the LEM.

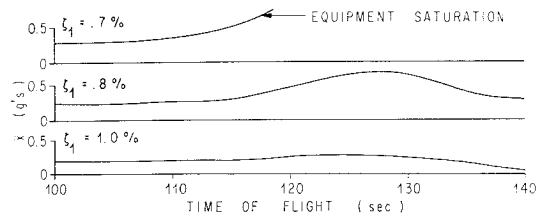

Fig. 8 Effect of varying first longitudinal modal damping on LEM acceleration.

Lowering the first longitudinal modal frequency causes the LOX suction line resonant frequency to coalesce with the longitudinal frequency at a later flight time where the modal mass and influence coefficients are again not as critical, resulting in less longitudinal response. The LEM lateral resonance, however, fails to coincide with this lower longitudinal frequency, and no lateral response occurs.

Figure 8 shows the longitudinal LEM response acceleration for various values of the first longitudinal generalized damping. The response is extremely sensitive to small variations in structural damping, being neutrally stable for 1% damping and strongly unstable for 0.7% damping (or less).

Figure 9 is a plot of the peak lateral and longitudinal LEM acceleration values as a function of the lateral LEM frequency. In the lateral direction, the system is highly sensitive to the lateral LEM frequency; the longitudinal LEM acceleration shows some sensitivity, but not to the degree that the lateral does. A sharp resonance between the longitudinal oscillation and the lateral LEM is necessary to have significant lateral responses.

Results of the same type are presented in Fig. 10 for the sensitivity of the system to varying the longitudinal LEM

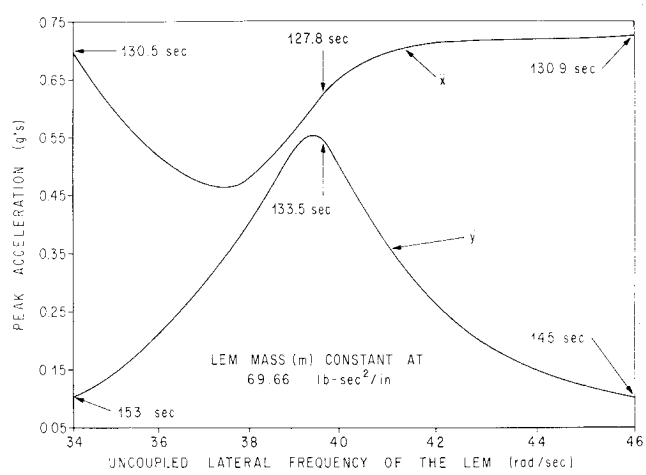

Fig. 9 Effect of lateral LEM frequency on longitudinal lateral coupling.

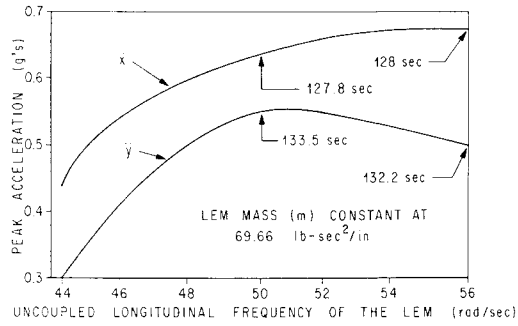

Fig. 10 Sensitivity of longitudinal/lateral coupling to longitudinal LEM frequency.

frequency. Since the longitudinal LEM mode is not in resonance but is being driven by the first longitudinal mode, the sharp tuning seen in Fig. 9 for the lateral LEM frequency, which is in resonance, will not be evident, as borne out by Fig. 10. A corresponding change in both lateral and longitudinal response should occur simultaneously as the LEM longitudinal frequency is varied, since this mode serves as a coupling mode.

Varying the cross-coupling term between longitudinal and lateral LEM modes had some effect on longitudinal responses (Fig. 11), reducing it in amplitude as the coupling increases. The increase in lateral response was more pronounced as the coupling increased. The reduction in longitudinal response is caused by the transfer of energy from the longitudinal to the lateral oscillation. This energy exchange takes energy from the longitudinal oscillations, thus reducing the longitudinal amplitude as the lateral oscillation builds up.

Changing the damping of the lateral LEM mode significantly changed the lateral LEM response, but virtually did not affect the longitudinal oscillation problem (Fig. 12). At the same time, increasing the longitudinal LEM mode damping reduced both the longitudinal and lateral response equally (Fig. 12). This provides additional evidence that the longitudinal mode is driving the lateral mode.

Including the accumulator model, discussed earlier, in the simulation, had the effect of lowering the resonant frequency at the LOX suction line to about 2 Hz. This caused a complete decoupling of the propulsion modes from the first longitudinal structural mode. The removal of the forcing function has eliminated the dangerous lateral responses.

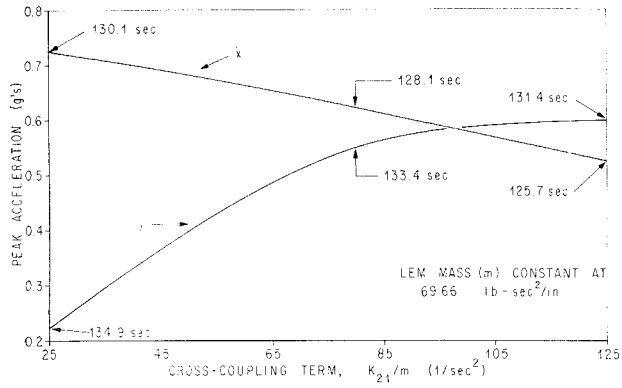

Fig. 11 Sensitivity of longitudinal/lateral coupling to LEM cross-coupling term.

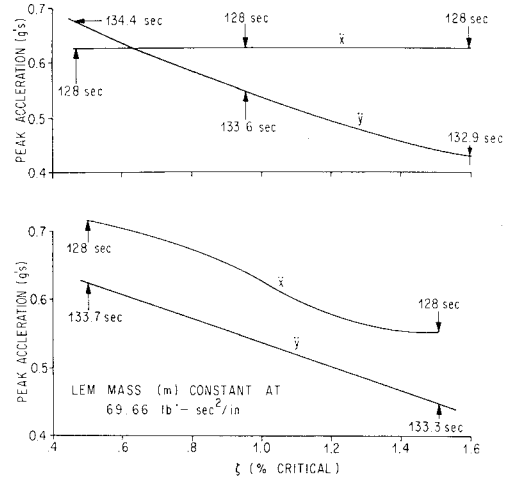

Fig. 12 Sensitivity of longitudinal/lateral coupling to lateral (top) and longitudinal (bottom) LEM mode damping.

Conclusions

This paper has shown the value of simulation to verify vehicle responses or to explain flight anomalies for over-all system analysis.

Coupling between longitudinal and lateral vehicle requires a coupling mechanism, a forcing function, and sharp tuning of frequencies. These conditions were present on AS-502: 1) the off-center mounting of the LEM ascent and descent stages provided the coupling mechanism, 2) the longitudinal oscillation (POGO) provided the forcing function, and 3) the LEM lateral frequency coalescence with the POGO provided the fine tuning.

The system response showed a high sensitivity to small parametric changes. Major contributing factors to the observed instability of the system were frequency tuning, phase shift between oscillatory modes, and amplification of oscillation disturbances in certain oscillatory loops (loop gain). These are functions of structural damping, influence coefficients, modal mass, modal frequencies, and propulsion system parameters. The high sensitivity of the system stability to these variables indicates the need for a detailed analysis for each individual vehicle.

References

[1] Martin Co., Denver Colo., "Dynamic Analysis of Longitudinal Oscillations of SM-68B Stage 1 (Pogo)," CR-4-71 (BSD TR 65-179), Contract AF04 (647)-576, March 1964, Ballistic Systems Div., Air Force Systems Command.

[2] Rubin, S., "Longitudinal Instability of Liquid Rockets Due to Propulsion Feedback (Pogo)," *Journal of Spacecraft and Rockets*, Vol. 3, No. 8, Aug. 1966, pp. 1188–1195.

[3] "Engine System Transfer Functions for Support of S-V Vehicle Longitudinal Stability (Pogo) Analysis Program," R-6829, NASA Contract NASw-16, March 8, 1967, Rocketdyne Div., Canoga Park, Calif.

[4] "Current Transfer Functions for F-1 Engine Block I (SA-501) Block II (SA-502)," NASA letter 68 RC 76666, June 19, 1968, Rocketdyne Div., Canoga Park, Calif.